Research Article

Static, dynamic and natural frequency analyses of functionally graded carbon nanotube annular sector plates resting on viscoelastic foundation

Masoud Babaei[1] · **Kamran Asemi**[2]

Received: 19 March 2020 / Accepted: 24 August 2020 / Published online: 9 September 2020

Abstract
In this paper, static, dynamic and natural frequency responses of composite annular sector plate with carbon nanotubes (CNTs) reinforcements resting on viscoelastic foundation are investigated. The carbon nanotubes are considered to have uniform or functionally graded pattern in the plate thickness. Kelvin-voight model is used to model the viscoelastic foundation. To model the problem, Hamilton principle based on first shear deformation plate theory and finite element method are applied. The mechanical properties of annular sector plate composed of CNTs and polymer matrix are evaluated by using the rule of mixtures. The numerical results are obtained for investigating the effect of various factors such as distribution and volume fraction of CNTs, boundary conditions, stiffness and damping coefficients of viscoelastic foundation and sector angles on natural frequency, static and dynamic transient responses of the plate.

Keywords FGCNT · Annular sector plate · FEM · FSDT · Natural frequency · Transient and static responses

1 Introduction

The specific mechanical properties of carbon nanotubes (CNTs) lead to utilize it instead of common reinforcements in composite structures. Because of great mechanical properties of the functionally graded carbon nanotube reinforced composite (FG-CNTRC) structures, many studies are conducted to investigate the responses of these structures, which some of them are reviewed here. Singh and Bhar [1] studied vibration characteristics of CNTRC plates by using the higher-order shear deformation theory (HSDT). Shen [2] investigated nonlinear static bending of FGCNT plate with simply supported boundary conditions under different transverse loads in thermal surroundings. Tornabene et al. [3] studied the linear static response of nanocomposite plates and shells reinforced by agglomerated CNTs based on several HSDTs. Zhu et al. [4] presented a numerical procedure based on finite element method for the natural frequency and static bending analyses of FGCNT plates for various boundary conditions by applying the first order shear deformation plate theory (FSDT). Lei et al. [5] studied the natural frequency and static bending responses of rectangular plates by applying element-free Ritz method and plate theories. Nonlinear vibration of CNT-RC plates based on a HSDT theory in thermal surroundings was studied by Wang and Shen [6]. They used perturbation technique to solve the obtained governing equations. Ansari et al. [7] performed natural frequency analysis of FG-CNTRC quadrilateral plates in thermal surroundings by using elasticity theory. The vibration characteristics of composite plates with FGCNT layers with arbitrary quadrilateral shape by using the FSDT and the differential quadrature method (DQM) were studied by Malekzadeh and Zarei [8]. Malekzadeh and Heydarpour

✉ Kamran Asemi, K.asemi@iau-tnb.ac.ir; Masoud Babaei, masoudbabaei@eyc.ac.ir | [1]Department of Mechanical Engineering, University of Eyvanekey, Eyvanekey, Semnan, Iran. [2]Department of Mechanical Engineering, Islamic Azad University, Tehran North Branch, Tehran, Iran.

[9] presented the natural frequency and static bending responses of simply supported composite plates with FGCNTRC layers by applying the Navier-layer wise and DQ methods. Natarajan et al. [10] used HSDT and normal deformable plate theory for static and natural frequency analysis of FGCNT plate and sandwich plates containing face sheets reinforced with CNTs. Alibeigloo and Emtehani [11] studied the natural frequency and static bending behavior of FGCNT rectangular plates under transverse uniform pressure for various boundary conditions by using DQM. Based on von-Karman assumptions and HSDT plate theory, nonlinear dynamic bending behavior of FGCNT plate supported on elastic medium in thermal surroundings were investigated by Wang and Shen [12]. Alibeigloo [13] by using an analytical solution based on theory of elasticity studied static bending response of FGCNT plate with piezoelectric layers. Phung-Van et al. [14] by using HSDT and isogeometric analysis methods studied static and dynamic bending response of the FGCNT plates with various essential boundary conditions.

Literature review shows the existence of a large number of researches on the response of FGCNTRC beams and rectangular plates. However, circular, sector, annular and annular sector plates are used in different engineering structures to sustain different static and dynamic loads. Hence, it is necessary to investigate response of these FGCNT structures under static and dynamic loads to satisfy the design requirements. In the literature, analyses correspond to FGCNT circular, annular and annular sector plates are limited in number. For example, Keleshteri et al. [15] and Mohammadzadeh-Keleshteri et al. [16] by using FSDT plate theory, von Karman starin-displacement assumptions, Hamilton principle and the generalized DQM studied the nonlinear vibration response of FGCNT annular sector plates with piezoelectric layers. Zhong et al. [17] based on FSDT and by using weak form approach and Ritz-variational energy method investigated vibration analysis of FGCNT annular and sector plates.

The literature review illustrates that a detailed study including; static, dynamic and free vibration analyses of FGCNT annular sector plate have not been investigate so far. Therefore, in this paper, static, dynamic and natural frequency behavior of composite FGCNT annular sector plates resting on viscoelastic foundation is investigated. In Sect. 2, geometry of plate resting on Kelvin-voight viscoelastic foundation and material properties of CNTRC are presented. The CNTs are considered to have uniform or functionally graded distributions in the plate thickness. The mechanical properties of composite annular sector plate composed of CNTs and a polymer matrix are evaluated by using the rule of mixtures. Then, the governing equations based on FSDT are derived and, finite element method is used to solve the governing equation of FGCNT plate. A 4-node two-dimensional element with 20 degree of freedom is applied to mesh the domain. In Sect. 3, first, static response of FGCNT annular sector plate have been verified by using data of a FGCNT square plate, and then, the effects of different factors such as distribution and volume fraction of CNTs, different boundary conditions, stiffness and damping coefficients of viscoelastic foundation and sector angles on natural frequency, static and transient dynamic responses of the plate have been studied.

2 Theoretical formulations

2.1 Description of the Geometry

An FGCNT annular sector plate resting on viscoelastic foundation with thickness h, angle of sector θ0, inner and outer radii R0 and R1 is considered (Fig. 1). The cylindrical coordinates r, θ and z at the mid-plane of the plate are used.

2.2 Material properties of CNTRC

In this study, the idea of FGMs is implemented to the nanocomposite structures reinforced by CNTs with low CNTs volume fractions. The carbon nanotubes are considered to have uniform or FG distributions in the plate thickness. UD-CNTRC denotes the uniform distribution of CNTs and FGX, FGO and FGV-CNTRC show the FG patterns of CNTs

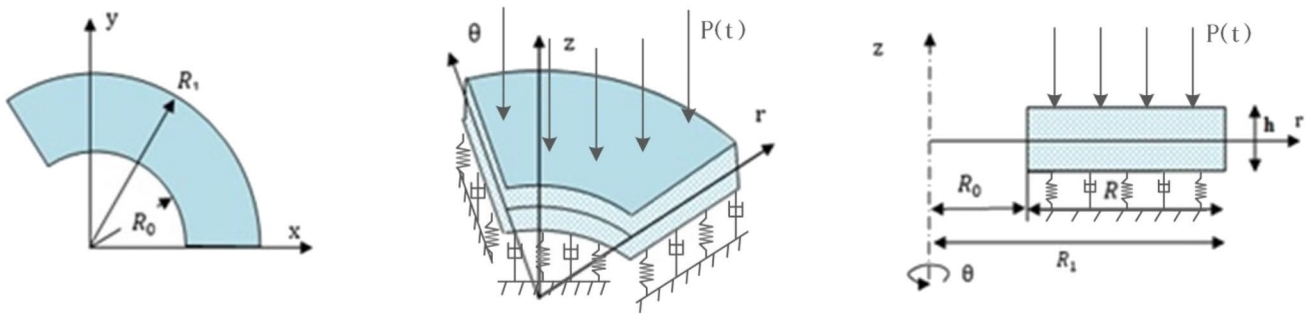

Fig. 1 Description of geometry and coordinate system of FGCNTRC annular sector plate

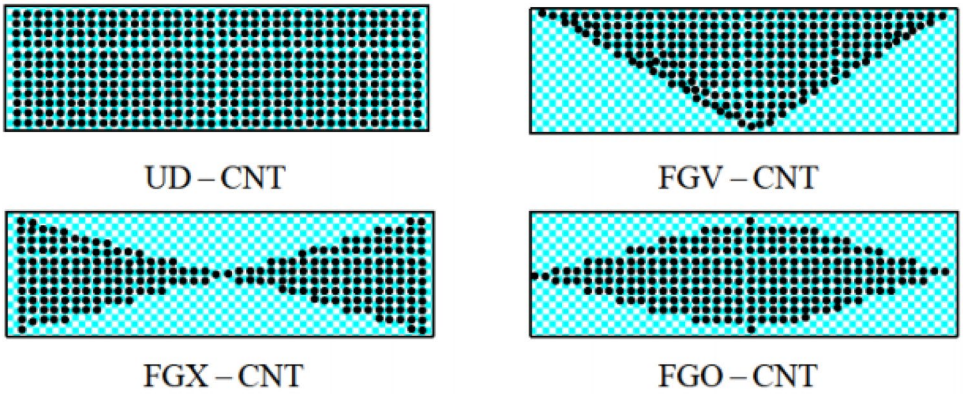

Fig. 2 Different kinds of CNTs distribution

through the plate thickness (Fig. 2). The mechanical properties of CNTs are considered to be size-dependent and are estimated from molecular dynamics (MD) simulations. The mechanical properties of FG CNTRCs are obtained by using a micromechanical model in which the CNTs efficiency parameter is obtained from the MD simulation with the results estimated from the rule of mixture [2]. The effective material properties may be estimated by Mori–Tanaka scheme or the rule of mixture. The Mori–Tanaka scheme is applicable to nanoparticles and the rule of mixture is simple and convenient to apply for predicting the overall material properties and responses of the structures. Thus, in this study, the effective mechanical properties of plate, mixtures of isotropic polymeric matrix and CNTs are evaluated by using the rule of mixtures [18] as shown in Eq. (1). In this model, it is assumed that both CNTs and polymer are very well-bonded and equally strained [2].

$$\begin{aligned} \rho &= V_{CN}\rho^{CN} + V_m\rho^m \\ E_{11} &= \eta_1 V_{CN}E_{11}^{CN} + V_m E^m \\ \frac{\eta_2}{E_{22}} &= \frac{V_{CN}}{E_{22}^{CN}} + \frac{V_m}{E^m}, \frac{\eta_3}{G_{12}} = \frac{V_{CN}}{G_{12}^{CN}} + \frac{V_m}{G^m} \\ \upsilon_{12} &= V_{CN}\upsilon_{12}^{CN} + V_m\upsilon^m \end{aligned} \tag{1}$$

where $E_{11}^{CN}, E_{22}^{CN}, G_{12}^{CN}, \upsilon_{12}^{CN}$ are modulus of elasticity, shear modulus and Poisson's ratio of carbon nanotubes, respectively. Also, E^m, G^m and υ^m are the same properties of isotropic polymer matrix. ρ^m and ρ^{CN} are the mass density of matrix and CNTs, respectively. V_{CN} is the volume fraction of CNTs, and V_m is the volume fraction of polymer matrix ($V_{CN} + V_m = 1$). V_{CN} for different distribution of CNTs are shown in Table 1. CNTs efficiency parameters η_i, $i = 1, 2, 3$ are given in Table 2 [19, 20].

2.3 Governing equations

According to the FSDT plate theory, the displacement components of annular sector plate are considered as [21]:

Table 1 Mathematical representation of CNT distributions

CNTs distribution	V_{CN}
UD CNT	V_{CN}^*
FG-X CNT	$4V_{CN}^* \frac{\lvert z\rvert}{h}$
FG-VCNT	$V_{CN}^*\left(1 + 2\frac{\lvert z\rvert}{h}\right)$
FG-OCNT	$2V_{CN}^*\left(1 - 2\frac{\lvert z\rvert}{h}\right)$

Table 2 CNTs efficiency parameters for different values of V_{CN}^*

Efficiency parameter	$V_{CN}^* = 0.11$	$V_{CN}^* = 0.14$	$V_{CN}^* = 0.17$
η_1	0.149	0.150	0.149
η_2	0.934	0.941	1.381
η_3	0.934	0.941	1.381

$$\begin{aligned} u(r,\theta,z) &= u_0(r,\theta) + z\varphi_r(r,\theta) \\ v(r,\theta,z) &= v_0(r,\theta) + z\varphi_r(r,\theta) \\ w(r,\theta,z) &= w_0(r,\theta) \end{aligned} \tag{2}$$

In Eq. (2), u, v, w, are displacement components along the r, θ and z directions, respectively, while u_0, v_0, w_0 are the same at the mid-plane. Also, φ_r and φ_θ are respectively normal transverse rotations around r and θ. The corresponding strains related to the displacement field are defined as follows:

$$\begin{aligned} &\varepsilon_r = \varepsilon_r^0 + zk_r^k, \varepsilon_\theta = \varepsilon_\theta^0 + zk_\theta^k \\ &\gamma_{r\theta} = \gamma_{r\theta}^0 + zk_{r\theta}, \gamma_{rz} = \gamma_{rz}^0, \gamma_{\theta z} = \gamma_{\theta z}^0 \end{aligned} \tag{3}$$

where

$$\varepsilon_r^0 = \frac{\partial u_0}{\partial r}, \varepsilon_\theta^0 = \frac{u_0}{r} + \frac{1}{r}\frac{\partial v_0}{\partial \theta}$$
$$k_r = \frac{\partial \varphi_r}{\partial r}, k_\theta = \frac{1}{r}\frac{\partial \varphi_\theta}{\partial \theta} + \frac{\varphi_r}{r}, k_{r\theta} = \frac{\partial \varphi_\theta}{\partial r} + \frac{1}{r}\frac{\partial \varphi_r}{\partial \theta} - \frac{\varphi_\theta}{r}$$
$$\gamma_{rz}^0 = \frac{\partial w}{\partial r} + \varphi_r, \gamma_{\theta z}^0 = \frac{1}{r}\frac{\partial w}{\partial \theta} + \varphi_\theta \frac{\partial w}{\partial \theta} + \varphi_\theta, \gamma_{r\theta}^0 = \frac{\partial v_0}{\partial r} + \frac{1}{r}\frac{\partial u_0}{\partial \theta} - \frac{v_0}{r} \tag{4}$$

The matrix form of the strain field is as follows

$$\begin{bmatrix} \varepsilon_r \\ \varepsilon_\theta \\ \gamma_{r\theta} \end{bmatrix} = \begin{Bmatrix} \varepsilon_r^0 \\ \varepsilon_\theta^0 \\ \gamma_{r\theta}^0 \end{Bmatrix} + z\begin{Bmatrix} k_r \\ k_\theta \\ k_{r\theta} \end{Bmatrix}$$

$$= \begin{bmatrix} \frac{\partial}{\partial r} & 0 & 0 & z\frac{\partial}{\partial r} & 0 \\ \frac{1}{r} & \frac{1}{r}\frac{\partial}{\partial \theta} & 0 & z\frac{1}{r} & \frac{z}{r}\frac{\partial}{\partial \theta} \\ \frac{1}{r}\frac{\partial}{\partial \theta} & \frac{\partial}{\partial r} - \frac{1}{r} & 0 & \frac{z}{r}\frac{\partial}{\partial \theta} & z\left(\frac{\partial}{\partial r} - \frac{1}{r}\right) \end{bmatrix} \begin{bmatrix} u_0 \\ v_0 \\ w_0 \\ \varphi_r \\ \varphi_\theta \end{bmatrix} = d_1 Q$$

$$\begin{Bmatrix} \gamma_{rz}^0 \\ \gamma_{\theta z}^0 \end{Bmatrix} = \begin{bmatrix} 0 & 0 & \frac{\partial}{\partial r} & 1 & 0 \\ 0 & 0 & \frac{1}{r}\frac{\partial}{\partial \theta} & 0 & 1 \end{bmatrix} \begin{bmatrix} u_0 \\ v_0 \\ w_0 \\ \varphi_r \\ \varphi_\theta \end{bmatrix} = d_2 Q$$

where

$$Q = \begin{bmatrix} u_0 \\ v_0 \\ w_0 \\ \varphi_r \\ \varphi_\theta \end{bmatrix}, d_1 = \begin{bmatrix} \frac{\partial}{\partial r} & 0 & 0 & z\frac{\partial}{\partial r} & 0 \\ \frac{1}{r} & \frac{1}{r}\frac{\partial}{\partial \theta} & 0 & z\frac{1}{r} & \frac{z}{r}\frac{\partial}{\partial \theta} \\ \frac{1}{r}\frac{\partial}{\partial \theta} & \frac{\partial}{\partial r} - \frac{1}{r} & 0 & \frac{z}{r}\frac{\partial}{\partial \theta} & z\left(\frac{\partial}{\partial r} - \frac{1}{r}\right) \end{bmatrix},$$

$$d_2 = \begin{bmatrix} 0 & 0 & \frac{\partial}{\partial r} & 1 & 0 \\ 0 & 0 & \frac{1}{r}\frac{\partial}{\partial \theta} & 0 & 1 \end{bmatrix},$$

$$\begin{Bmatrix} \varepsilon_r^0 \\ \varepsilon_\theta^0 \\ \gamma_{r\theta}^0 \end{Bmatrix} = \begin{bmatrix} \frac{\partial}{\partial r} & 0 & 0 & 0 & 0 \\ \frac{1}{r} & \frac{1}{r}\frac{\partial}{\partial \theta} & 0 & 0 & 0 \\ \frac{1}{r}\frac{\partial}{\partial \theta} & \frac{\partial}{\partial r} - \frac{1}{r} & 0 & 0 & 0 \end{bmatrix} \begin{bmatrix} u_0 \\ v_0 \\ w_0 \\ \varphi_r \\ \varphi_\theta \end{bmatrix} = d_3 Q$$

$$\begin{Bmatrix} k_r \\ k_\theta \\ k_{r\theta} \end{Bmatrix} = \begin{bmatrix} 0 & 0 & 0 & \frac{\partial}{\partial r} & 0 \\ 0 & 0 & 0 & \frac{1}{r} & \frac{1}{r}\frac{\partial}{\partial \theta} \\ 0 & 0 & 0 & \frac{1}{r}\frac{\partial}{\partial \theta} & \left(\frac{\partial}{\partial r} - \frac{1}{r}\right) \end{bmatrix} \begin{bmatrix} u_0 \\ v_0 \\ w_0 \\ \varphi_r \\ \varphi_\theta \end{bmatrix} = d_4 Q \tag{5}$$

where

$$d_3 = \begin{bmatrix} \frac{\partial}{\partial r} & 0 & 0 & 0 & 0 \\ \frac{1}{r} & \frac{1}{r}\frac{\partial}{\partial \theta} & 0 & 0 & 0 \\ \frac{1}{r}\frac{\partial}{\partial \theta} & \frac{\partial}{\partial r} - \frac{1}{r} & 0 & 0 & 0 \end{bmatrix}, d_4 = \begin{bmatrix} 0 & 0 & 0 & \frac{\partial}{\partial r} & 0 \\ 0 & 0 & 0 & \frac{1}{r} & \frac{1}{r}\frac{\partial}{\partial \theta} \\ 0 & 0 & 0 & \frac{1}{r}\frac{\partial}{\partial \theta} & \left(\frac{\partial}{\partial r} - \frac{1}{r}\right) \end{bmatrix},$$

The relation between stress and strain in an orthotropic structure is as:

$$\begin{Bmatrix} \sigma_r \\ \sigma_\theta \\ \tau_{r\theta} \end{Bmatrix}^k = \begin{bmatrix} C_{11} & C_{12} & 0 \\ C_{12} & C_{22} & 0 \\ 0 & 0 & C_{66} \end{bmatrix}^k \begin{Bmatrix} \varepsilon_r \\ \varepsilon_\theta \\ \gamma_{r\theta} \end{Bmatrix}^k$$
$$\begin{Bmatrix} \tau_{rz} \\ \tau_{\theta z} \end{Bmatrix}^k = \begin{bmatrix} C_{44} & 0 \\ 0 & C_{55} \end{bmatrix}^k \begin{Bmatrix} \gamma_{rz} \\ \gamma_{\theta z} \end{Bmatrix}^k \tag{6}$$

$$C_{11} = \frac{E_{11}}{1 - v_{12}v_{21}}, C_{12} = \frac{v_{12}E_{22}}{1 - v_{12}v_{21}} = \frac{v_{21}E_{11}}{1 - v_{12}v_{21}}$$
$$C_{22} = \frac{E_{22}}{1 - v_{12}v_{21}}, C_{44} = G_{13}, C_{55} = G_{23}, C_{66} = G_{12}$$

The resultants of moment and force are given by integrating the stress components through the z direction:

$$\begin{Bmatrix} N_r \\ N_\theta \\ N_{r\theta} \end{Bmatrix} = \int_{-h/2}^{h/2} \begin{bmatrix} \sigma_r \\ \sigma_\theta \\ \tau_{r\theta} \end{bmatrix} dz, \quad \begin{Bmatrix} M_r \\ M_\theta \\ M_{r\theta} \end{Bmatrix} = \int_{-h/2}^{h/2} \begin{bmatrix} \sigma_r \\ \sigma_\theta \\ \tau_{r\theta} \end{bmatrix} z dz \tag{7}$$

$$\begin{Bmatrix} Q_r \\ Q_\theta \end{Bmatrix} = K^2 \int_{-h/2}^{h/2} \begin{bmatrix} \tau_{rz} \\ \tau_{\theta z} \end{bmatrix} dz = K^2 \sum_{K=1}^{n} \int_{zk-1}^{zk} \begin{Bmatrix} \tau_{rz} \\ \tau_{\theta z} \end{Bmatrix}^{(k)} dz$$

where K = 5/6 is the shear correction factor.

By the integral from Eq. (7) along the thickness:

$$\begin{bmatrix} N_r \\ N_\theta \\ N_{r\theta} \\ M_r \\ M_\theta \\ M_{r\theta} \\ Q_r \\ Q_\theta \end{bmatrix} = \begin{bmatrix} A_{11} & A_{12} & 0 & B_{11} & B_{12} & 0 & 0 & 0 \\ A_{12} & A_{22} & 0 & B_{12} & B_{22} & 0 & 0 & 0 \\ 0 & 0 & A_{66} & 0 & 0 & B_{66} & 0 & 0 \\ B_{11} & B_{12} & 0 & D_{11} & D_{12} & 0 & 0 & 0 \\ B_{12} & B_{22} & 0 & D_{12} & D_{22} & 0 & 0 & 0 \\ 0 & 0 & B_{66} & 0 & 0 & D_{66} & 0 & 0 \\ 0 & 0 & 0 & 0 & 0 & 0 & K^2A_{44} & 0 \\ 0 & 0 & 0 & 0 & 0 & 0 & 0 & K^2A_{55} \end{bmatrix} \begin{Bmatrix} \varepsilon_r^0 \\ \varepsilon_\theta^0 \\ \gamma_{r\theta}^0 \\ k_r \\ k_\theta \\ k_{r\theta} \\ \gamma_{rz}^0 \\ \gamma_{\theta z}^0 \end{Bmatrix} \tag{8}$$

where:

$$(A_{ij}, B_{ij}, D_{ij}) = \int_{-\frac{h}{2}}^{\frac{h}{2}} C_{ij}(1, z, z^2) dz \tag{9}$$

The strain and kinetic energies for the annular sector plate is expressed as

$$\delta U = \delta U_1 = \frac{1}{2}\iiint \varepsilon^T \sigma dV = \iint \left\{ \begin{matrix} \varepsilon_r^0 + N_\theta \varepsilon_\theta^0 + N_{r\theta}\gamma_{r\theta}^0 + M_r K_r + M_\theta K_\theta + \\ M_{r\theta}K_{r\theta} + Q_r \gamma_{rz} + Q_\theta \gamma_{\theta z} \end{matrix} \right\} r dr d\theta$$
$$= \int \left(\left(\left(d_3 Q\right)^T A^T + \left(d_4 Q\right)^T B^T \right)(d_3 \delta Q) + \left(\left(d_3 Q\right)^T B^T + \left(d_4 Q\right)^T D^T \right)(d_4 \delta Q) \right.$$
$$\left. + \left(d_2 Q\right)^T e^T \left(d_2 \delta Q\right) \right) r dr d\theta \tag{10}$$
$$\delta T = \int_{-\frac{h}{2}}^{\frac{h}{2}} \rho(\ddot{u}\delta u + \ddot{v}\delta v + \ddot{w}\delta w) dV$$

where:

$$\begin{cases} \delta u = \delta u_0 + z\delta\varphi_r \\ \delta v = \delta v_0 + z\delta\varphi_\theta \\ \delta w = \delta w_0 \end{cases} \qquad \begin{cases} \ddot{u} = \frac{\partial^2 u_0}{\partial t^2} + z\frac{\partial^2 \varphi_r}{\partial t^2} \\ \ddot{v} = \frac{\partial^2 v_0}{\partial t^2} + z\frac{\partial^2 \varphi_\theta}{\partial t^2} \\ \ddot{w} = \frac{\partial^2 w_0}{\partial t^2} \end{cases} \tag{11}$$

$$T = \int \int_{-\frac{h}{2}}^{\frac{h}{2}} \rho \left(\left(\frac{\partial^2 u_0}{\partial t^2} + z\frac{\partial^2 \varphi_r}{\partial t^2} \right)\left(\delta u_0 + z\delta\varphi_r\right) + \left(\frac{\partial^2 v_0}{\partial t^2} + z\frac{\partial^2 \varphi_\theta}{\partial t^2} \right)\left(\delta v_0 + z\delta\varphi_\theta\right) + \frac{\partial^2 w_0}{\partial t^2}\delta w_0 \right) dz dA$$

By substituting Eqs. (10), (11) in Hamilton principle, we have:

$$\int_{t_1}^{t_2} \left[\iint_{-\frac{h}{2}}^{\frac{h}{2}} \rho \left(\left(\frac{\partial^2 u_0}{\partial t^2} + z\frac{\partial^2 \varphi_r}{\partial t^2} \right)\left(\delta u_0 + z\delta\varphi_r\right) + \left(\frac{\partial^2 v_0}{\partial t^2} + z\frac{\partial^2 \varphi_\theta}{\partial t^2} \right)\left(\delta v_0 + z\delta\varphi_\theta\right) \right.\right.$$
$$\left. + \frac{\partial^2 w_0}{\partial t^2}\delta w_0 \right) dz dA$$
$$+ \int \left(\left(\left(d_3 Q\right)^T A^T + \left(d_4 Q\right)^T B^T \right)(d_3 \delta Q) + \left(\left(d_3 Q\right)^T B^T + \left(d_4 Q\right)^T D^T \right)(d_4 \delta Q) \right.$$
$$\left.\left. + \left(d_2 Q\right)^T e^T \left(d_2 \delta Q\right) \right) r dr d\theta - \delta W \right] dt = 0 \tag{12}$$

δW is virtual work of external forces, where the plate is subjected to a transverse pressure P_z is as following equation:

$$\delta W = \int P_z \delta w_0 r dr d\theta \tag{13}$$

2.4 Finite element model of governing equations

Finite element method is used to solve the governing equation of FGCNT plate. A 4-node two-dimensional element with 20 degree of freedom is applied to mesh the solution domain (Fig. 3). Also, a local-coordinate system (ξ, η) is used to express shape functions.

The relationship between the natural and the global coordinates is as [22, 23]:

$$\xi = \frac{2r - a^{(e)} - b^{(e)}}{\left(b^{(e)} - a^{(e)}\right)}, \quad \eta = \frac{2\left(\theta - \theta_c\right)}{\beta^{(e)}} \tag{14}$$

where $-1 \le \xi,\ \eta \le 1$ are through the r and θ directions. $a^{(e)}$, $b^{(e)}$ and $\beta^{(e)}$ are the inner and outer radii and angle of sector of element, respectively. Also, θ_c is the circumferential coordinate of center of element.

The shape functions in the natural coordinates and the displacement vector of element are defined as follow

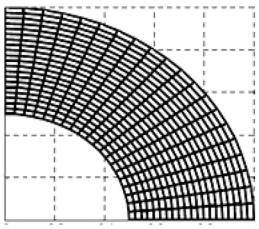

Fig. 3 The schematic of the meshed annular sector plate and the natural coordinates

$$\begin{Bmatrix} \Psi_i \\ \Psi_j \\ \Psi_k \\ \Psi_m \end{Bmatrix} = \frac{1}{4}\begin{Bmatrix} (1+\xi)(1-\eta) \\ (1+\xi)(1+\eta) \\ (1-\xi)(1+\eta) \\ (1-\xi)(1-\eta) \end{Bmatrix} \tag{15}$$

$$Q^{(e)} = \left(\begin{pmatrix} \Psi_1 & \cdots & 0 \\ \vdots & \ddots & \vdots \\ 0 & \cdots & \Psi_1 \end{pmatrix} \cdots \begin{pmatrix} \Psi_4 & \cdots & 0 \\ \vdots & \ddots & \vdots \\ 0 & \cdots & \Psi_4 \end{pmatrix}\right)\begin{Bmatrix} u_{01} \\ v_{01} \\ w_{01} \\ \varphi_{r1} \\ \varphi_{\theta 1} \\ \vdots \\ u_{04} \\ v_{04} \\ w_{04} \\ \varphi_{r4} \\ \varphi_{\theta 4} \end{Bmatrix} = \Psi q(e) \tag{16}$$

where Ψ_n, n = 1, 2, 3, 4 are the shape functions, and Ψ is the matrix of shape functions. $u_{0i}, v_{0i}, w_{0i}, \varphi_{ri}$ and $\varphi_{\theta i}$ are nodal degrees of freedom and are approximated as

$$u_0 = \sum_{i=1}^{4} \Psi_i U_{0i}, v_0 = \sum_{i=1}^{4} \Psi_i V_{0i}, w_0 = \sum_{i=1}^{4} \Psi_i W_{0i}$$
$$\varphi_r = \sum_{i=1}^{4} \Psi_i \theta_{ri}, \varphi_\theta = \sum_{i=1}^{4} \Psi_i \theta_{\theta i} \tag{17}$$

Substituting Eq. (17) in Eq. (12) can be rewritten as

$$\int_{\Omega_0^e} \Big[\Big(\left(d_3\Psi\right)^T A^T d_3\Psi + \left(d_4\Psi\right)^T B^T d_3\Psi + \left(d_3\Psi\right)^T B^T d_4\Psi + \left(d_4\Psi\right)^T D^T d_4\Psi + \left(d_2\Psi\right)^T e^T d_2\Psi\Big)d + \Psi^T I\Psi\ddot{q} - \Psi^T P\Big] r dr d\theta = 0 \tag{18}$$

where $P = \begin{bmatrix} 0 \\ 0 \\ P_z \\ 0 \\ 0 \end{bmatrix}, d_2\Psi = B_2, d_3\Psi = B_3, d_4\Psi = B_4$

By sorting the above equation, the following equation is obtained for the each annular sector element:

$$\left(k_1 + k_2 + k_3\right)^{(e)} q^{(e)} + M^e \ddot{q}^{(e)} = F^e \tag{19}$$

Finally, after sum of the stiffness, mass and force element matrices, the finite element equations of the FGCNT plate is as

$$\left(k_1 + k_2 + k_3\right) q + M\ddot{q} = F \tag{20}$$

For the case that the plate is resting on the Kelvin-voight linear viscoelastic foundation, the relationship between force per unit area and deflection can be calculated according to the following equation [24]:

$$P_v = k_w w + c_d \frac{\partial w}{\partial t} \tag{21}$$

where k_w is the elastic coefficient of the foundation in terms of (N/m^3), and C_d is the damping coefficient of the foundation in terms of ($N\ s/m^3$). Therefore, in this case, by adding the effects of viscoelastic foundation on the plate, the governing Eq. (20) can be rearranged as:

$$\left(k_1 + k_2 + k_3 + k_4\right) q + M\ddot{q} + C\dot{q} = F \tag{22}$$

where k_4 is the stiffness matrix due to the elastic properties of the foundation, and C is the damping matrix due to damping property of foundation. The mass, stiffness, damping and force matrices are given in "Appendix".

The considered essential boundary conditions of plate are as:

All edges clamped (CCCC):

$$u_0,\ v_0,\ w_0,\ \varphi_r,\ \varphi_\theta = 0 \quad at(r, 0), \left(r, \theta_0\right), (a, \theta), (b, \theta) \tag{23}$$

Clamped radial edges (FCFC):

$$u_0,\ v_0,\ w_0,\ \varphi_r,\ \varphi_\theta = 0 \quad at\ (r,0),\left(r,\theta_0\right) = 0 \tag{24}$$

Clamped circumferential edges (CFCF):

$$u_0,\ v_0,\ w_0,\ \varphi_r,\ \varphi_\theta = 0 \quad at\ (a,\theta),(b,\theta) \tag{25}$$

Simply supported edges (SSSS):

$$\begin{aligned} &u_0,\ w_0 = 0 \quad at\ (a,\theta),(b,\theta)\\ &v_0,\ w_0 = 0 \quad at\ (r,0),\left(r,\theta_0\right) \end{aligned} \tag{26}$$

Finally, Newmark integeration method [25] is applied to solve the Eq. (22) with respect to time. The natural frequency analysis of the plate converts to the solution of the eigen value problem as

$$\left(\left(k_1+k_2+k_3+k_4\right)-M\omega^2\right)q = 0 \tag{27}$$

where ω is the circular natural frequency and q is the vibration mode shapes.

3 Results and discussions

In this part, results of static, natural frequency and dynamic transient responses of FGCNT annular sector plate resting on viscoelastic foundation have been presented. The effect of various boundary conditions, stiffness and damping coefficients of viscoelastic foundation, CNT distributions, volume fraction of CNTs, slenderness ratio and sector angle have been studied. The mechanical and geometrical

Table 5 Effects of V_{CN} on $\tilde{W} = w_0/h$, P = 1 MPa, CCCC, θ_0 = 30°, 60°,120°, 240° (a = 1 m, b = 2 m, h = 0.1 m)

V_{CN}	UD	FGX	FGV	FGO
θ_0 = 30°				
0.11	0.01912	0.018101	0.019946	0.021201
0.14	0.017971	0.01698	0.018575	0.01971
0.17	0.012107	0.011253	0.012561	0.013505
θ_0 = 60°				
0.11	0.022728	0.021478	0.024307	0.026021
0.14	0.021169	0.020111	0.022345	0.023683
0.17	0.014413	0.013501	0.015361	0.016473
θ_0 = 120°				
0.11	0.02257	0.021329	0.024067	0.025754
0.14	0.021048	0.019975	0.022151	0.023489
0.17	0.01431	0.013383	0.015204	0.016315
θ_0 = 240°				
0.11	0.022808	0.021556	0.024299	0.02599
0.14	0.021272	0.020188	0.022382	0.023733
0.17	0.014461	0.013525	0.015347	0.016471

Table 3 Mechanical and geometrical properties of FGCNT annular sector plate

Geometrical properties (mm)			
a(m)	b(m)	θ_0	h(m)
1	2	30°, 60°, 120°, 240°	0.1, 0.05
Mechanical properties of polymeric core (MPa)			
E_{11}^{CN}(TPa)	E_{22}^{CN}(TPa)		G_{12}^{CN}(TPa)
5.6466	7.08		1.9445
υ_{12}^{CN}	$\rho^{CN}\left(\frac{Kg}{m^3}\right)$		E^m(GPa)
0.175	1400		2.1
G^m(GPa)	υ^m		$\rho^m\left(\frac{Kg}{m^3}\right)$
$\frac{E^m}{2(1+\upsilon^m)}$	0.34		1150

Table 4 Effect of V_{CN} on the $\tilde{W} = w_0/h$ of FGCNT square plate with all edges clamped (CCCC) subjected to an uniform pressure P = 0.1 MPa (a = 200 m, b = 200.2 m, h = 0.02 m, α = 0.001 rad)

V_{CN}	UD (Present)	UD [4]	FGX (Present)	FGX [4]	FGV (Present)	FGV [4]	FGO (Present)	FGO [4]
0.11	0.002226	0.002228	0.002106	0.002109	0.002353	0.002351	0.002509	0.002512
0.14	0.002083	0.002087	0.001974	0.001979	0.002176	0.002182	0.002307	.002313
0.17	0.0014108	0.001412	0.0013176	0.001318	0.001484	.001483	0.001593	0.001595

Table 6 Effects of different boundary conditions on $\tilde{W} = w_0/h$, P = 1 MPa, $\theta_0 = 120°$ (a = 1 m, b = 2 m, h = 0.05 m), $V_{CN} = 0.11$

	UD	FGX	FGV	FGO
CCCC	0.1328	0.114223	0.157748	0.184754
CFCF	0.13016	0.111324	0.155998	0.183737
FCFC	4.56E+02	4.27E+02	4.51E+02	4.80E+02
SCSC	0.352556	0.263195	0.378349	0.60904
SSSS	0.357795	0.267416	0.383524	0.616172

properties of FGCNT annular sector plate are presented in Table 3.

3.1 Static analysis

3.1.1 verification

In this section, static response of FGCNT annular sector plate have been verified by using data of a FGCNT square plate [4]. Table 4 shows the effect of V_{CN} and different distributions of nanotubes on the non-dimensional central deflection $\tilde{W} = w_0/h$ of FGCNT square plates with CCCC edges. Therefore, the sector angle is assumed as a small value $\theta_0 = 0.001$ rad, and inner and outer radiuses of plate are chosen as large values: b = 200 m, a = 200.2 m and h = 0.02 m. These geometric dimensions lead to nearly a square plate with length-to-thickness ratio of 10:1. Also, the material properties are considered as previous section. Comparison between results in Table 4 shows excellent agreement between them.

3.1.2 Static analysis of FGCNT annular sector plate

In this part, static response of FGCNT annular sector plate without foundation under a transverse pressure P = 1 MPa is investigated. The effects of V_{CN} on the non-dimensional central deflection $\tilde{W} = w_0/h$ are shown in Table 5. Also, the effects of CNTs distribution and sector angle have been investigated. Table 5 denotes that V_{CN} has great influence on the deflection of plate. Increasing V_{CN} from 0.11 to 0.17 leads to more than 36% decrease in the deflection. This is because that by increasing V_{CN}, stiffness of plate enhances. Also, results show that the maximum and minimum deflection belong to the FGO and FGX distributions, respectively. Therefore, it can be deduced that CNTs distribution close to upper and lower surface of plate are more appropriate than those distributions concentrated on near the mid-plane for enhancing the overall stiffness of plate. Also, results present that as the sector angle increases from 30° to 60°, central deflection of plate is also increases, and for 60° to 240°, it is almost identical. Table 6 shows the effect of different boundary conditions on the non-dimensional central deflection. In this case: $\theta_0 = 120°$, h = 0.05 m, $V_{CN} = 0.11$. Results denote that the maximum and minimum non-dimensional central deflection is related to FCFC and CFCF boundary conditions, respectively. Also, comparisons between Tables 5 and 6

Table 7 Effects of V_{CN} on $\tilde{\omega} = \omega(a^2/h)\sqrt{\rho^m/E^m}$ of FGCNT square plate with all edges clamped (CCCC) (a = 200 m, b = 200.2 m, h = 0.02 m, $\theta_0 = 0.001$ rad)

V_{CN}	Mode No.	UD (Present)	UD [4]	FGX (Present)	FGX [4]	FGV (Present)	FGV [4]	FGO (Present)	FGO [4]
0.11	1	17.597	17.625	18.058	18.083	17.181	17.211	16.675	16.707
	2	22.898	23.041	23.461	23.606	22.678	22.818	22.117	22.253
	3	33.02	33.529	33.760	34.338	32.932	33.070	32.232	32.378
	4	33.601	33.729	34.344	34.464	32.988	33.552	32.304	32.857
	5	36.877	37.011	37.404	37.400	36.390	36.528	35.668	35.809
	6	37.267	37.317	37.654	38.084	37.397	37.437	37.410	37.447
0.14	1	18.108	18.127	18.577	18.642	17.773	17.791	17.291	17.311
	2	23.438	23.572	24.107	24.369	23.285	23.413	22.659	22.782
	3	33.683	34.252	34.649	35.224	33.718	34.101	32.867	33.411
	4	34.537	34.650	35.303	35.410	33.983	34.275	33.317	33.441
	5	37.805	37.921	38.136	38.121	37.422	37.538	36.672	36.788
	6	37.931	37.972	38.673	39.095	38.129	38.159	38.143	38.169
0.17	1	21.973	22.011	22.711	22.804	21.506	21.544	20.795	20.833
	2	28.618	28.801	29.685	30.023	28.443	28.613	27.498	27.651
	3	41.293	42.015	42.845	43.287	41.254	41.431	40.121	40.501
	4	41.965	42.132	43.129	43.572	41.425	42.119	40.315	40.781
	5	46.076	46.250	47.016	47.009	45.624	45.796	44.533	44.699
	6	46.627	46.694	47.424	47.969	47.007	47.055	47.032	47.071

Table 8 Effects of V_{CN} on natural frequency (HZ) of FGCNT annular sector plates with all edges clamped (CCCC), $\theta_0 = 30°, 60°, 120°$ (a = 1 m, b = 2 m, h = 0.1 m)

V_{CN}	Mode No.	$\theta_0 = 30°$				$\theta_0 = 60°$				$\theta_0 = 120°$			
		UD	FGX	FGV	FGO	UD	FGX	FGV	FGO	UD	FGX	FGV	FGO
0.11	1	414.0709	424.8366	406.4293	395.0324	356.1417	365.718	346.0358	335.2815	350.7767	360.2913	340.2497	329.4741
	2	622.8128	636.7897	619.9632	606.6531	386.5901	396.7111	378.218	367.2895	353.3996	362.8785	343.1937	332.5199
	3	747.5764	764.1869	734.2616	718.7409	459.1608	470.74	453.3992	441.6231	360.7854	370.3323	351.1939	340.5717
	4	917.0845	935.6225	909.6212	892.6586	571.9117	585.5306	568.6482	555.5276	376.1527	385.9747	367.5115	356.8078
	5	917.898	935.7547	918.297	902.2937	611.9101	613.9557	613.8404	614.0227	402.2749	412.6433	394.8796	383.8987
	6	955.3279	958.8783	958.6299	959.0382	709.4366	725.5742	694.0373	678.8873	440.545	451.7265	434.5567	423.0923
0.14	1	425.2758	436.9167	419.2672	407.7313	367.1464	376.4193	358.8644	349.0664	361.8372	370.893	353.1792	343.5119
	2	636.2213	653.7074	634.8686	619.1431	397.5272	408.084	390.8218	380.1467	364.383	373.4985	356.012	346.3464
	3	767.8257	785.4492	756.8785	741.5991	470.5211	483.8607	466.2548	453.5369	371.6768	381.0814	363.8556	354.0263
	4	935.7511	959.4862	933.0031	914.0536	584.5096	601.3809	582.6761	567.3346	386.9823	397.0589	380.0217	369.7371
	5	938.206	960.2731	937.8646	917.6334	622.8472	626.0416	625.9363	626.1208	413.1418	424.3466	407.325	396.229
	6	972.3647	977.6561	977.4079	977.846	726.1829	746.1148	716.858	702.6714	451.6235	464.366	447.1214	434.8913
0.17	1	517.1918	535.6097	509.112	491.9594	444.5471	459.0506	432.8315	418.5511	437.8083	451.9366	425.4963	411.4545
	2	778.666	806.6555	778.1418	754.2176	482.7562	499.4141	473.545	457.7668	441.1104	455.3581	429.2484	415.1786
	3	933.7924	960.7285	920.0408	898.2829	573.7256	594.9522	568.413	549.2946	450.3906	465.1414	439.3961	425.0191
	4	1146.257	1181.02	1141.208	1113.087	714.951	741.9199	713.5906	690.2741	469.6798	485.5619	460.0478	444.8877
	5	1148.028	1186.249	1153.394	1122.355	765.5937	771.701	771.5701	771.8824	502.4456	520.1964	494.6297	478.119
	6	1195.258	1205.272	1204.931	1205.703	885.9461	910.5946	869.2235	849.4093	550.421	570.6925	544.701	526.3387

Table 9 Effects of different boundary conditions on natural frequency (HZ) of FGCNT annular sector plates, $V_{CN} = 0.11$, α = 120° (a = 1 m, b = 2 m, h = 0.05 m)

	UD	FGX	FGV	FGO
CCCC	292.4447	314.5595	268.6749	248.7521
	293.5046	315.4782	269.9996	250.2419
	296.2584	318.0104	273.288	253.7785
	301.9806	323.4399	279.8957	260.7158
	312.1752	333.294	291.3862	272.5936
	328.3256	349.1003	309.2287	290.829
CFCF	292.1821	314.3537	268.3111	248.3308
	292.2684	314.4072	268.4323	248.4997
	292.7068	314.7207	269.0638	249.2696
	293.9415	315.7441	270.6855	251.113
	296.8584	318.3732	274.2532	254.9804
	302.7264	323.8925	281.1076	262.2048
FCFC	5.727783	5.920648	5.75792	5.585857
	15.68032	16.21052	15.75168	15.27689
	22.35516	23.09105	22.44172	21.7807
	30.67117	31.71775	30.78721	29.84659
	46.8389	48.40097	46.99846	45.59145
	50.31903	52.05301	50.45933	48.89582
SCSC	178.4713	204.7207	172.5659	135.9825
	180.8721	206.4446	175.0873	139.2347
	186.312	208.5048	180.775	146.3023
	196.5102	213.3126	191.3703	158.9719
	203.8926	222.5562	204.7382	178.6845
	213.1469	237.9885	208.5288	204.7657
SSSS	178.2625	204.7202	172.3487	135.7096
	179.9224	206.2592	174.0948	138.0196
	183.8586	207.6492	178.2273	143.2526
	191.6504	211.0679	186.3354	153.1441
	203.8921	218.0387	200.2373	169.3872
	205.0665	230.3476	204.682	193.0671

show that by decreasing the thickness of plate, deflection significantly is increased.

3.2 Natural frequency analysis

3.2.1 Verification

In this section, natural frequency of FGCNT annular sector plate has been validated by using data of FGCNT square plate [4]. Table 7 shows the effects of V_{CN} and distributions of carbon nanotubes on the non-dimensional natural frequency $\tilde{\omega} = \omega(a^2/h)\sqrt{\rho^m/E^m}$ of CNTRC square plates with CCCC edges. Geometric dimensions and the mechanical properties are considered same as the previous sections. Comparison between results in Table 7 shows excellent agreement between them.

3.2.2 Natural frequency analysis of FGCNT annular sector plate

In this part, free vibration analysis of FGCNT annular sector plate without foundation is investigated. Table 8 shows the effects of V_{CN} on the natural frequencies of CCCC plate. Also, the effects of CNTs distribution and sector angle have been investigated. Table 8 denotes that as V_{CN} increases, natural frequencies are increased. It should be noted that by enhancing V_{CN}, both of the stiffness and mass density of plate increases. However, the effect of CNTs on the stiffness of the structure is more considerable than the mass density. Therefore, the natural frequencies of plate are increased. Also, Table 8 denotes that minimum and maximum fundamental frequency belongs to the FGO and FGX distributions. Furthermore, results show that as the sector angle of plate increases, the fundamental frequency decreases. Table 9 shows the effects of different boundary conditions on natural frequencies of FGCNT annular sector plates for $V_{CN} = 0.11$, $\theta_0 = 120°$ and h = 0.05 m. Results show that the minimum natural frequencies are related to FCFC and fundamental frequencies of CCCC and CFCF boundary conditions and also fundamental frequencies of SSSS and SCSC boundary conditions are almost identical.

Figures 4, 5, 6 and 7 show the first six mode shapes of FGCNT annular sector plate for $\theta_0 = 30°$, 60°, 120° and 240°, respectively (FGV, $V_{CN} = 0.11$, a = 1 m, b = 2 m, h = 0.1 m, CCCC). Figures 8, 9, 10 show the first six mode shapes of FGCNT annular sector plate for FCFC, SSSS and SCSC boundary conditions, respectively. (FGV, $V_{CN} = 0.11$, a = 1 m, b = 2 m, h = 0.05 m, $\theta_0 = 120°$)

3.3 Transient vibration analysis

3.3.1 Transient analysis of plate without foundation

Transient vibration analysis of FGCNT annular sector plate without foundation is conducted, and the effect of the different distribution of CNTs and V_{CN} on time histories of centerpoint of plate are investigated (a = 1 m, b = 2 m, h = 0.1 m, $\theta_0 = 120°$, CCCC). The plate is under an impulsive loading (Eq. 28), and the plate is unloaded in t = 0.005 (s).

$$P_z = \begin{cases} 400t\left(\frac{MPa}{s}\right) & t \le 0.005 \\ 0 & t \ge 0.005 \end{cases} \quad (28)$$

Figure 11 shows the effects of V_{CN} on the time history of centerpoint of plate for UD distribution. This figure show that by increasing V_{CN}, the amplitude of transient vibration decreases and its frequency increases. Figure 12 shows the effect of different distributions of CNTs on time history of centerPoint of plate for $V_{CN} = 0.11$. It can be seen that the minimum and maximum amplitude of vibration is related

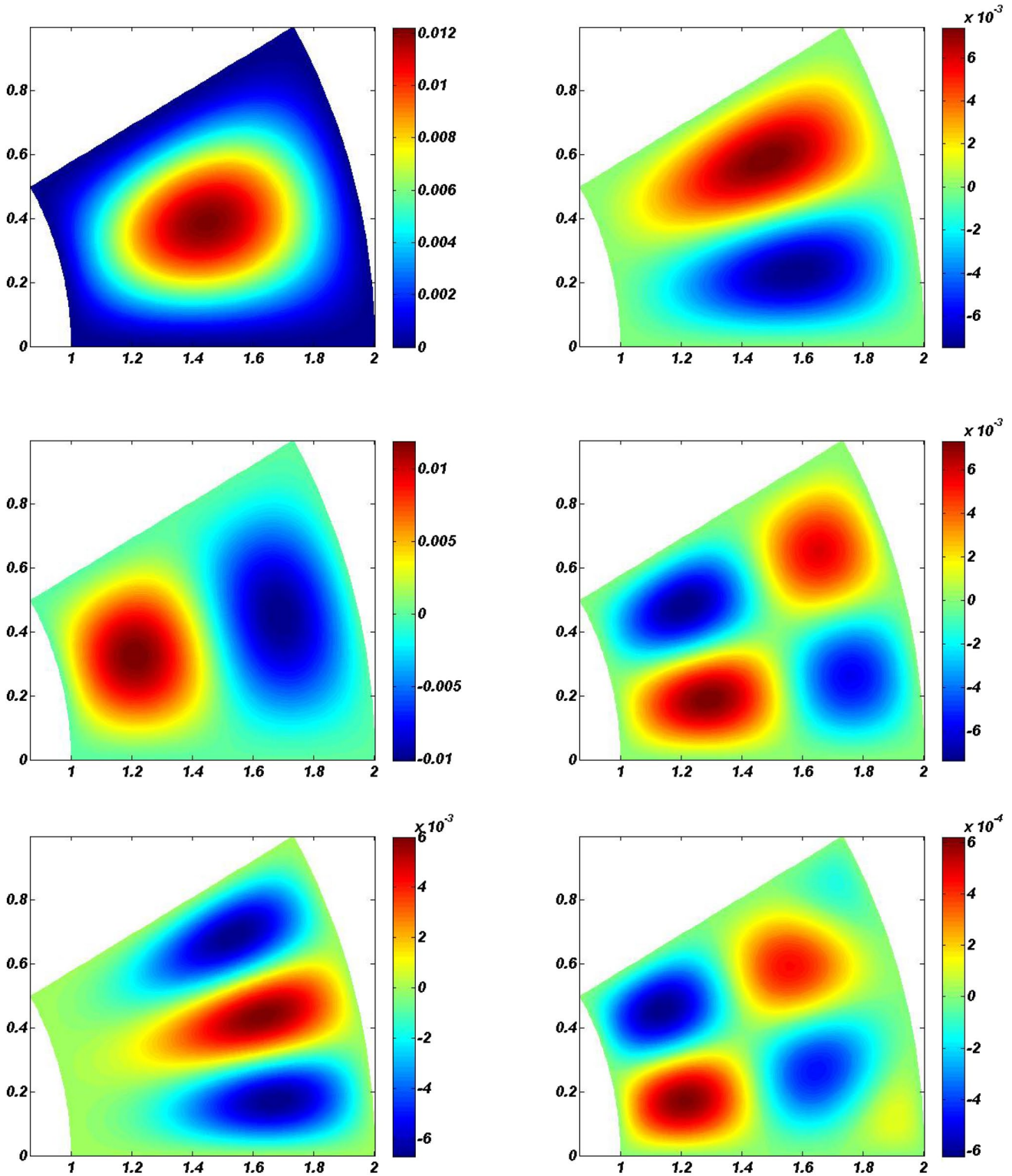

Fig. 4 The first six mode shapes of FGCNT annular sector plate (FGV, $V_{CN} = 0.11$, a = 1 m, b = 2 m, h = 0.1 m, $\theta_0 = 30°$, CCCC)

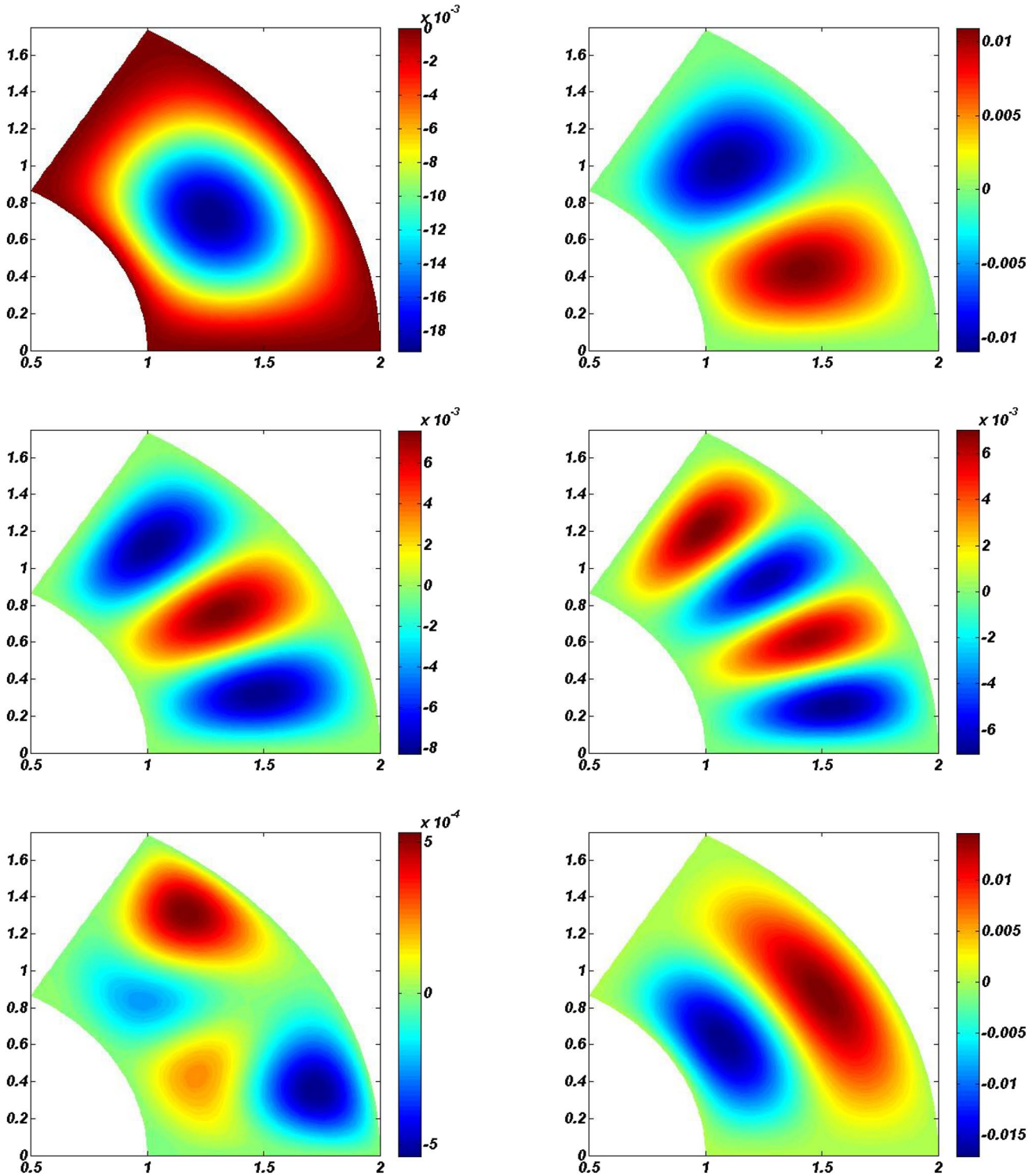

Fig. 5 The first six mode shapes of FGCNT annular sector plate (FGV, V_{CN} = 0.11, a = 1 m, b = 2 m, h = 0.1 m, θ_0 = 60°, CCCC)

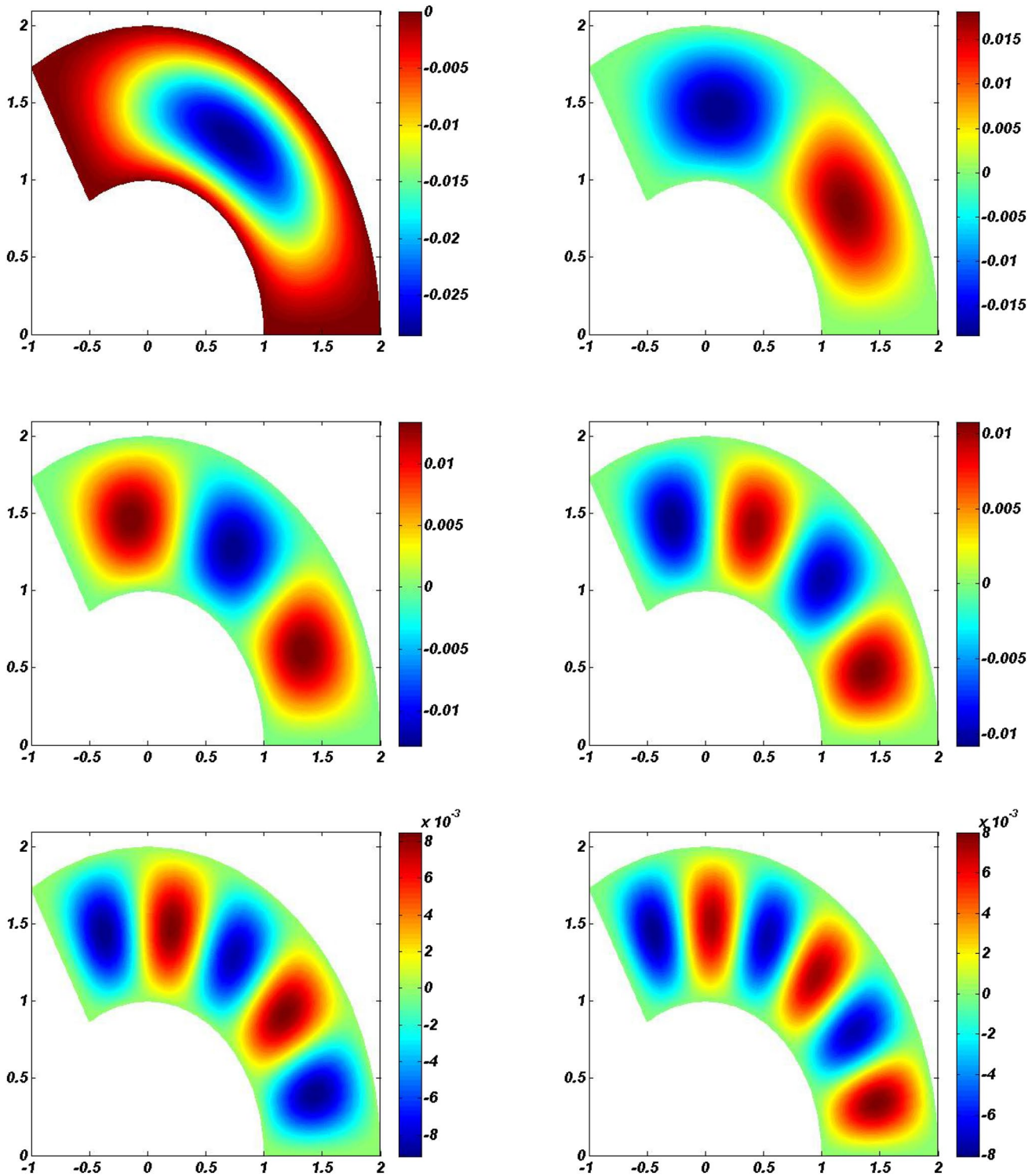

Fig. 6 The first six mode shapes of FGCNT annular sector plate (FGV, V_{CN} = 0.11, a = 1 m, b = 2 m, h = 0.1 m, θ_0 = 120°, CCCC)

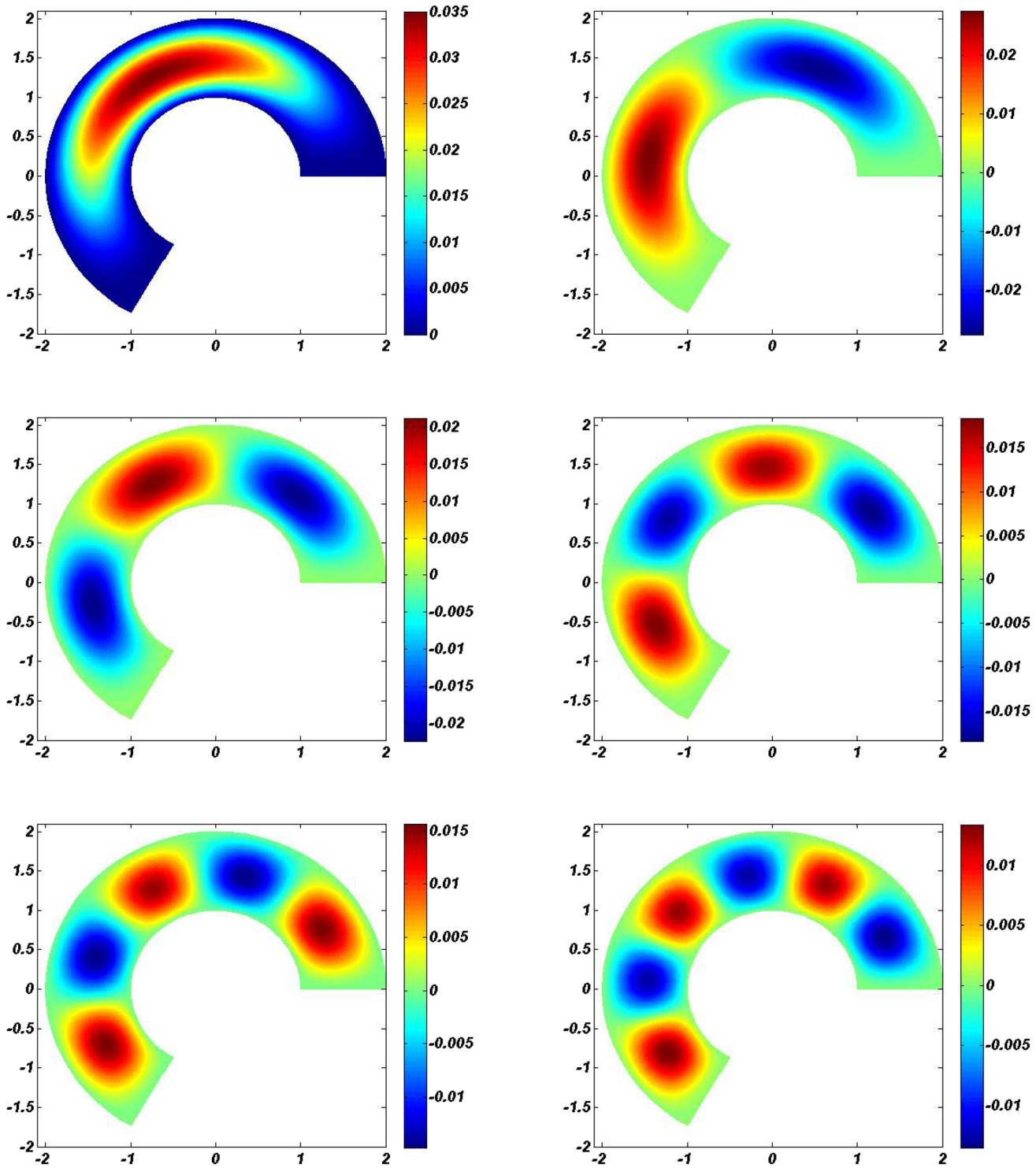

Fig. 7 The first six mode shapes of FGCNT annular sector plate (FGV, V_{CN} = 0.11, a = 1 m, b = 2 m, h = 0.1 m, θ_0 = 240°, CCCC)

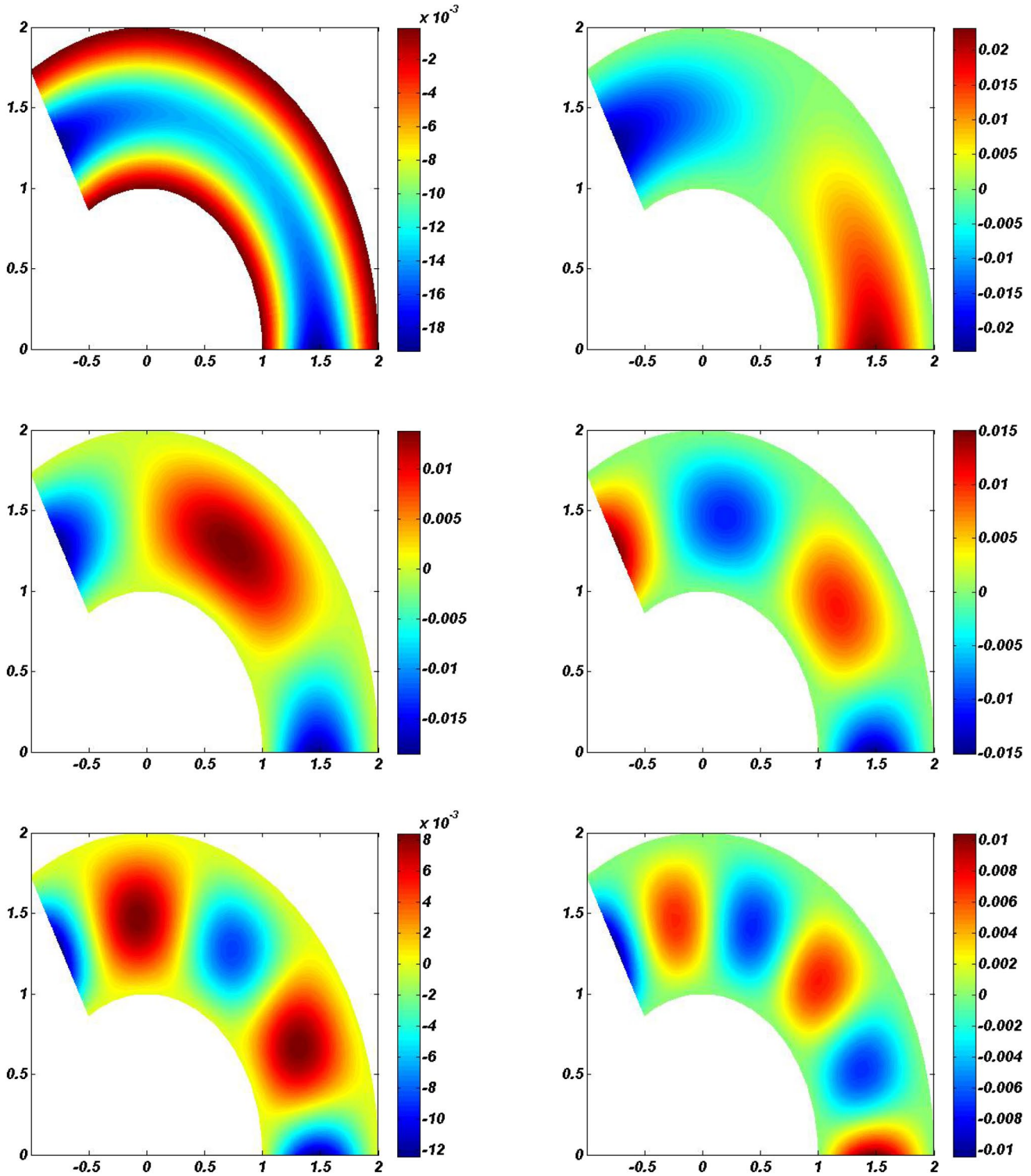

Fig. 8 The first six mode shapes of FGCNT annular sector plate (FGV, V_{CN} = 0.11, a = 1 m, b = 2 m, h = 0.05 m, θ_0 = 120°, FCFC)

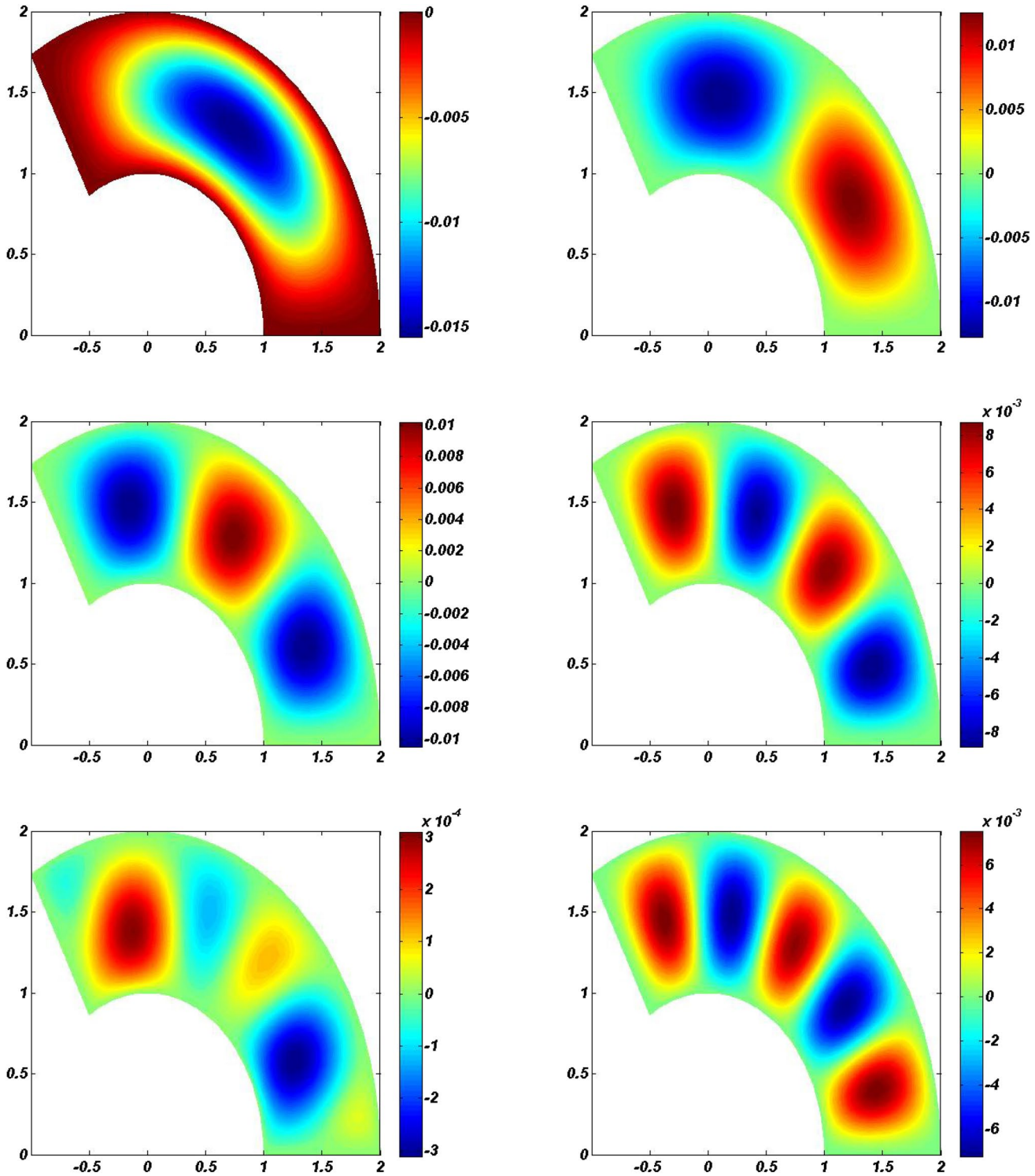

Fig. 9 The first six mode shapes of FGCNT annular sector plate (FGV, V_{CN} = 0.11, a = 1 m, b = 2 m, h = 0.05 m, θ_0 = 120°, SCSC)

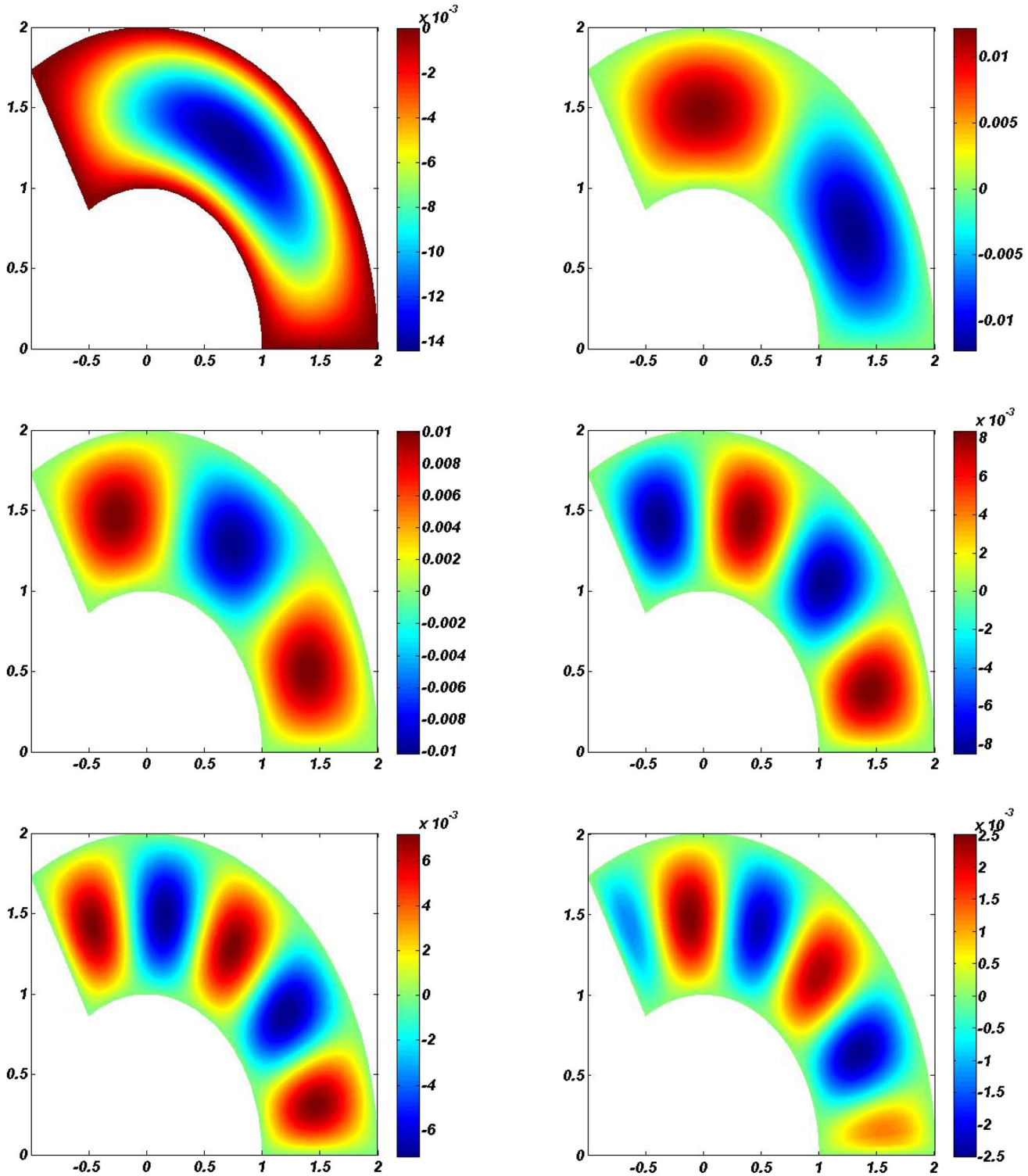

Fig. 10 The first six mode shapes of FGCNT annular sector plate (FGV, V_{CN} = 0.11, a = 1 m, b = 2 m, h = 0.05 m, θ_0 = 120°, SSSS)

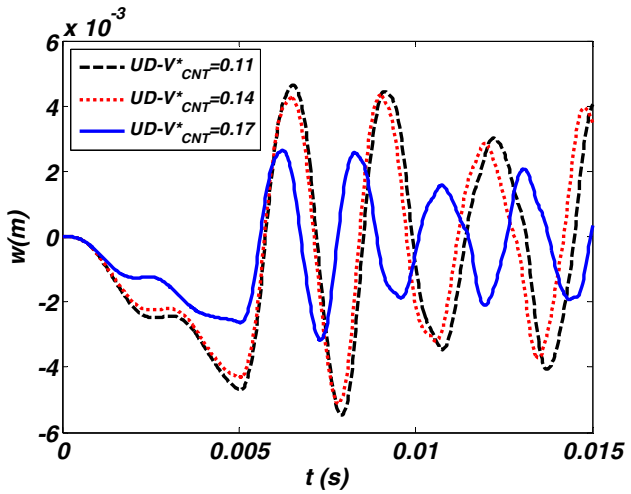

Fig. 11 The effect of V_{CN} on time history of centerpoint of plate (UD, a = 1 m, b = 2 m, h = 0.1 m, $\theta_0 = 120°$, CCCC)

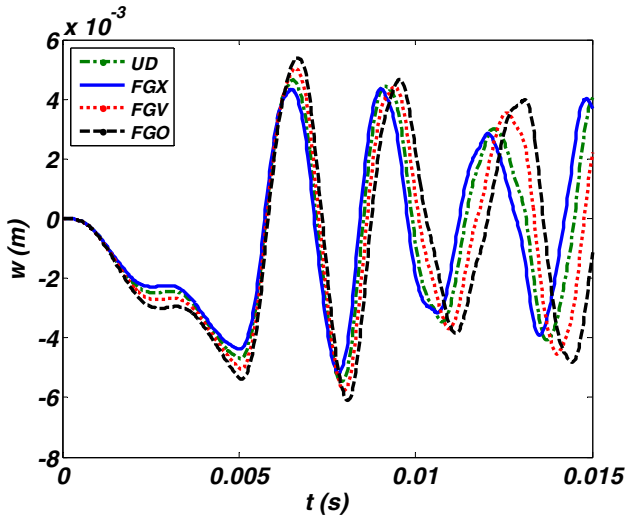

Fig. 12 The effect of different distribution of CNTs on time history of centerpoint of plate ($V_{CN} = 0.11$, a = 1 m, b = 2 m, h = 0.1 m, $\theta_0 = 120°$, CCCC)

to FGX and FGO distributions. Figure 13 shows the transient vibration behavior of FGCNT annular sector plate.

3.3.2 Transient analysis of plate resting on viscoelastic foundation

In this part, the effect of viscoelastic foundation on the transient behavior of plate is considered (a = 1 m, b = 2 m, h = 0.1 m, $\theta_0 = 120°$, CCCC, $V_{CN} = 0.11$, UD). The loading function is according to Eq. (28). Figure 14 show the effect of elastic coefficient of foundation on time history of centerpoint transverse displacement of plate. In this result, damping coefficient of the foundation is considered to be zero ($c_d = 0$). Result illustrates that by increasing the elastic coefficient of the foundation, the stiffness of plate increases, and consequently, amplitude of transverse displacement decreases significantly, and also, frequency of transient vibration increases. Figure 15 shows the effect of damping coefficient of foundation on time history of centerpoint transverse displacement of plate. In this result, elastic coefficient of the foundation is considered to be zero ($k_w = 0$). As it can be seen from this figure, by increasing damping of the foundation, amplitude of vibration diminishes and vibration of plate can be seen in three situations such as under-damped, critically-damped and over-damped.

4 Conclusions

A full comprehensive study about static, dynamic and natural frequency analyses of FGCNT annular sector plate has been investigated. A general solution based on FSDT in polar coordinate is presented that can be used for analyses of circular, annular and annular sector plates. Linear strain–displacement relationship is used to model the problem, and it is assumed that the plate is resting on simple linear Kelvin-voight viscoelastic foundation. Hamilton principle and finite element method have been used to derive the governing motion equations. A 4-node two-dimensional element with 20 degree of freedom is applied to mesh the domain. The influence of volume fraction of carbon and its distribution, different boundary conditions, damping and stiffness of viscoelastic foundation and sector angles on displacements and natural frequency of plate have been studied. Results show that volume fraction of CNTs has great effect on the deflection of plate, and increasing the V_{CN} from 0.11 to 0.17 leads to more than 36% decrease in the deflection. Also, the minimum and maximum displacements correspond to the FGX and FGO distributions, respectively. It means that CNTs distributions close to upper and lower surface of plate are more appropriate than those distribution concentrated on near the mid-plane for enhancing the overall stiffness of plate. Also, results denote that by increasing the V_{CN}, natural frequencies increases, and minimum and maximum fundamental frequency corresponds to the FGO and FGX distributions. Furthermore, by increasing damping of the foundation, amplitude of vibration decreases and vibration of plate can be seen in three situations such as under-damped, critically-damped and over-damped. For the future studies, applying higher order theories for thicker plates, large deflection analysis, and also investigating the effects of nonlinear foundations can be considered.

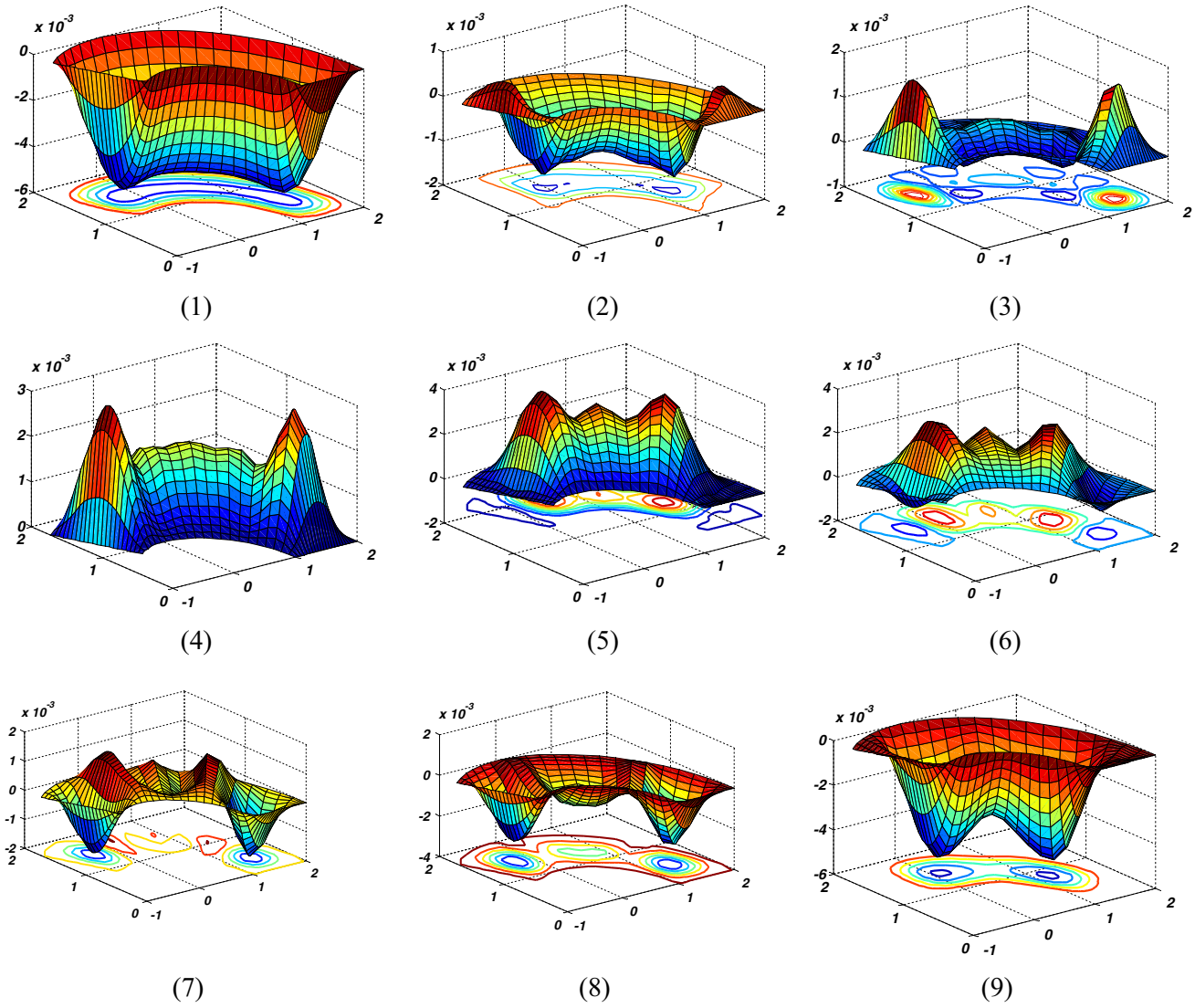

Fig. 13 Dynamic behavior of FGCNT plate (FGO, V_{CN}=0.11, a=1 m, b=2 m, h=0.1 m, θ_0=120°, CCCC (1) t=0.005 s, (2) t=0.005725 s, (3) t=0.00585 s, (4) t=0.005975 s, (5) 0.0071 s, (6) t=0.007225 s, (7) t=0.00735 s, (8) t=0.007475 s, (9) t=0.008475 s)

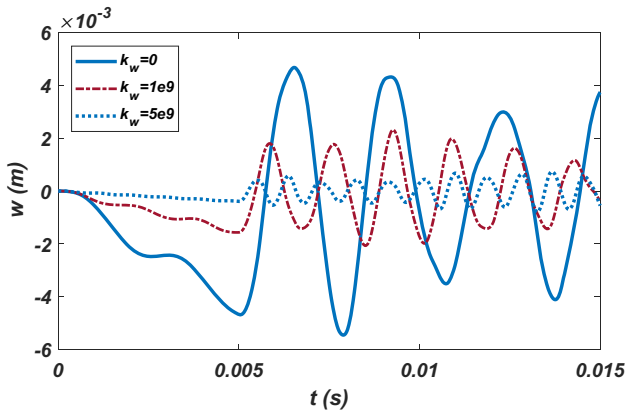

Fig. 14 The effect of different stiffness coefficient of viscoelastic foundation on time history of centerpoint of plate (V_{CN} = 0.11, UD, a = 1 m, b = 2 m, h = 0.1 m, $\theta_0 = 120°$, CCCC)

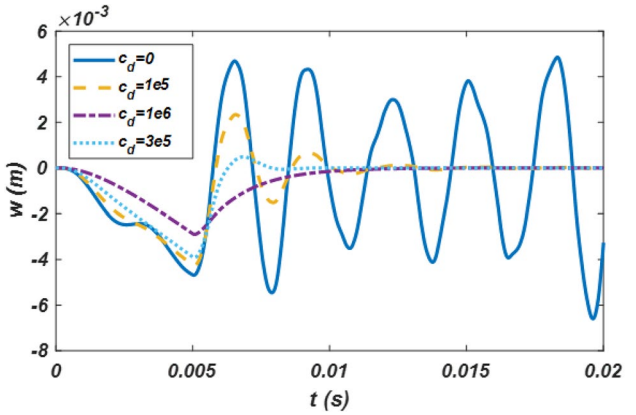

Fig. 15 The effect of different damping coefficient of viscoelastic foundation on time history of centerpoint of plate (V_{CN} = 0.11, UD, a = 1 m, b = 2 m, h = 0.1 m, $\theta_0 = 120°$, CCCC)

Compliance with ethical standards

Conflict of interest On behalf of all authors, the corresponding author states that there is no conflict of interest.

Appendix

$$M^e = \int_{\Omega_0^e} \Psi^t I \Psi r dr d\theta \tag{29}$$

$$k_1^e = \int_{\Omega_0^e} \left[B_3^T A^T + B_4^T B^T\right] B_3 r dr d\theta \tag{30}$$

$$k_2^e = \int_{\Omega_0^e} \left[B_3^T B^T + B_4^T D^T\right] B_4 r dr d\theta \tag{31}$$

$$k_3^e = \int_{\Omega_0^e} \left[B_2^T e^T B_2\right] r dr d\theta \tag{32}$$

$$k_4^e = \int_{\Omega_0^e} \left[\Psi^T k_w \Psi\right] r dr d\theta \tag{33}$$

$$F^e = \int_{\Omega_0^e} \Psi^T P r dr d\theta \tag{34}$$

$$C^e = \int_{\Omega_0^e} \Psi^T c_d \Psi r dr d\theta \tag{35}$$

I is a mass inertia matrix and is obtained from the following equation:

$$I = \begin{bmatrix} I_0 & 0 & 0 & I_1 & 0 \\ 0 & I_0 & 0 & 0 & I_1 \\ 0 & 0 & I_0 & 0 & 0 \\ I_1 & 0 & 0 & I_2 & 0 \\ 0 & I_1 & 0 & 0 & I_2 \end{bmatrix} \tag{36}$$

where $I_i, i = 0, 1, 2$ are

$$\begin{Bmatrix} I_0 \\ I_1 \\ I_2 \end{Bmatrix} = \int_{-\frac{h}{2}}^{\frac{h}{2}} \begin{Bmatrix} 1 \\ z \\ z^2 \end{Bmatrix} \rho dz \tag{37}$$

References

1. Singh AK, Bhar A (2019) Isogeometric FE analysis of CNT-reinforced composite plates: free vibration. SN Appl Sci 1(9):1010
2. Shen H (2009) Nonlinear bending of functionally graded carbon nanotube- reinforced composite plates in thermal environments. Compos Struct 91(1):9–19
3. Tornabene F, Fantuzzi N, Bacciocchi M (2017) Linear static response of nanocomposite plates and shells reinforced by agglomerated carbon nanotubes. Compos B Eng 115:449–476
4. Zhu P, Lei Z, Liew KM (2012) Static and free vibration analyses of carbon nanotube-reinforced composite plates using finite element method with first order shear deformation plate theory. Compos Struct 94:1450–1460
5. Lei ZX, Zhang LW, Liew KM (2015) Free vibration analysis of laminated FG-CNT reinforced composite rectangular plates using the kp-Ritz method. Compos Struct 127:245–259

6. Wang ZX, Shen HS (2011) Nonlinear vibration of nanotube-reinforced composite plates in thermal environments. Comput Mater Sci 50(8):2319–2330
7. Ansari R, Shahabodini A, Shojaei MF (2016) Vibrational analysis of carbon nanotube-reinforced composite quadrilateral plates subjected to thermal environments using a weak formulation of elasticity. Compos Struct 139:167–187
8. Malekzadeh P, Zarei A (2014) Free vibration of quadrilateral laminated plates with carbon nanotube reinforced composite layers. Thin-Walled Struct 82:221–232
9. Malekzadeh P, Heydarpour Y (2015) Mixed Navier-layerwise differential quadrature three-dimensional static and free vibration analysis of functionally graded carbon nanotube reinforced composite laminated plates. Meccanica 50:143–167
10. Natarajan S, Haboussi M, Manickam G (2014) Application of higherorder structural theory to bending and free vibration analysis of sandwich plates with CNT reinforced composite facesheets. Compos Struct 113:197–207
11. Alibeigloo A, Emtehani A (2015) Static and free vibration analyses of carbon nanotube-reinforced composite plate using differential quadrature method. Meccanica 50:61–76
12. Wang Z-X, Shen H-S (2012) Nonlinear dynamic response of nanotube-reinforced composite plates resting on elastic foundations in thermal environments. Nonlinear Dyn 70:735–754
13. Alibeigloo A (2013) Static analysis of functionally graded carbon nanotube-reinforced composite plate embedded in piezoelectric layers by using theory of elasticity. Compos Struct 95:612–622
14. Phung-Van P, Abdel-Wahab M, Liew K, Bordas S, Nguyen-Xuan H (2015) Isogeometric analysis of functionally graded carbon nanotube-reinforced composite plates using higher-order shear deformation theory. Compos Struct 123:137–149
15. Keleshteri MM, Asadi H, Wang Q (2017) Large amplitude vibration of FG-CNT reinforced composite annular plates with integrated piezoelectric layers on elastic foundation. Thin-Walled Struct 120:203–214
16. Mohammadzadeh-Keleshteri M, Asadi H, Aghdam MM (2017) Geometrical nonlinear free vibration responses of FG-CNT reinforced composite annular sector plates integrated with piezoelectric layers. Compos Struct 171:100–112
17. Zhong R, Wang Q, Tang J, Shuai C, Qin B (2018) Vibration analysis of functionally graded carbon nanotube reinforced composites (FG-CNTRC) circular, annular and sector plates. Compos Struct 194:49–67
18. Malekzadeh P, Dehbozorgi M (2016) Low velocity impact analysis of functionally graded carbon nanotubes reinforced composite skew plates. J Compstruct 01:045
19. Wang ZX, Xu J, Qiao P (2014) Nonlinear low-velocity impact analysis of temperature-dependent nanotube-reinforced composite plates. Compos Struct 108:423–434
20. Zhang LW, Cui W, Liew KM (2015) Vibration analysis of functionally graded carbn nanotube reinforced composite thick plates with elastically restrained edges. Int J Mech Sci 103:9–21
21. Timoshenko SP, Woinowsky-Krieger S (1959) Theory of plates and shells, 2nd edn. McGraw-Hill, New York
22. Asemi K, Salehi M (2018) Shear post buckling analysis of FGM annular sector plates based on three dimensional elasticity for different boundary conditions. Comput Struct 207:132–147
23. Babaei M, Hajmohammad MH, Asemi K (2020) Natural frequency and dynamic analyses of functionally graded saturated porous annular sector plate and cylindrical panel based on 3D elasticity. Aerospace Sci Technol 96:105524
24. Babaei M, Asemi K, Safarpour P (2019) Natural frequency and dynamic analyses of functionally graded saturated porous beam resting on viscoelastic foundation based on higher order beam theory. J Solid Mech 11(3):615–634
25. Zienkiewicz OC, Taylor RL, Zhu JZ (2005) The finite element method: its basis and fundamentals. Elsevier, New York